4038 J. Med. Chem. 2010, 53, 4038–4049
DOI: 10.1021/jm1001106

Journal of Medicinal Chemistry Article

Conserved Structural Motif for Recognizing Nicotinamide Adenine Dinucleotide in Poly(ADP-ribose) Polymerases and ADP-Ribosylating Toxins: Implications for Structure-Based Drug Design

Yu-Ming Lee,[†] C. Satheesan Babu,[‡] Yao Chi Chen,[‡] Milos Milcic,[‡] Yuanyuan Qu,[§] and Carmay Lim*[,‡,†]

[†]*Department of Chemistry, National Tsing Hua University, Hsinchu 300, Taiwan,* [‡]*Institute of Biomedical Sciences, Academia Sinica, Taipei 115, Taiwan, and* [§]*Department of Physics, Zhejiang University, Zhejiang, P.R.C.*

Received January 26, 2010

The ADP-ribosylating toxins (ADPRTs) and poly(ADP-ribose) polymerases (PARPs) are two important drug−target protein families. Although the $Y-X_{10}-Y$ motif for the diphtheria toxin group and the STS motif for the other ADPRTs have been found to recognize the NAD^+ substrate, it is not known (i) if these two different motifs share any structural similarity, (ii) the key forces/residues contributing to NAD^+ binding, and (iii) if they recognize the same or different NAD^+ conformations. Here, we show that even though the different toxin groups and PARPs share insignificant sequence identity, they share a similar 3D structure shaped like a scorpion (the "scorpion" motif) whose first three and last residues interact mainly with the NAD^+ nicotinamide ring via van der Waals forces. This locally conserved structure binds the nicotinamide mononucleotide moiety in a structurally conserved ringlike conformation. The biological implications/applications of locally conserved structures for toxins/PARPs and the nicotinamide mononucleotide are discussed.

Introduction

The ADP-ribosylating toxins (ADPRTs[a]) and poly ADP-ribose polymerases (PARPs) are two main classes of nicotinamide adenine dinucleotide (NAD, Figure 1a) metabolizing enzymes that catalyze the breakup of NAD into nicotinamide and ADP-ribose and the subsequent transfer of ADP-ribose to a target protein (see Scheme 1).[1] The PARPs are ubiquitous enzymes in most eukaryotes and are known to function in post-translational protein modifications where the ADP-ribose moiety is transferred from NAD onto specific substrates. Seventeen putative PARP sequences have been identified in the human genome, including at least six enzymes: PARP-1, PARP-2, PARP-3, PARP-4, PARP-5a (tankyrase-1, TNKS-1), and PARP-5b (tankyrase-2, TNKS-2).[2−4] They are involved in genome protection, transcriptional regulation, DNA damage sensor and repair, energy metabolism, cell proliferation, cell differentiation, and apoptosis.[1,2,4−6] Excessive activation of PARPs can result in depletion of NAD^+ and ATP in the cell and lead to inflammatory injury, cell dysfunction, and ultimately necrotic cell death.[7] PARP-1 knockout mice have been found to develop normally, suggesting that PARP-1 may not be necessary for survival.[8] The overexpression of PARPs have been linked to survivability from genotoxic stress of cancer cells and resistance to DNA-damaging agents.[9] Inhibition of PARPs can enhance the effects of anticancer therapies by preventing cancer cells from repairing DNA damage, thereby promoting apoptosis.[10−14] Recently, potent PARP inhibitors such as 1 (ABT-888,[15] Figure 1b) for metastatic melanoma[16] and **2** (AG014699,[17] Figure 1c) for breast cancer, ovarian cancer, and melanoma[18] have completed phase II trials.[13,19] Therefore, PARPs are promising targets for drug development aimed at inflammation, degenerative and vascular diseases, ischemia, and cancer therapy.[2,9,19,20]

The ADPRTs are a large family of dangerous and potentially lethal toxins secreted by pathogenic bacteria, which inactivate the function of their human target proteins. On the basis of structure-based multiple-sequence alignments, the ADPRT family has been classified into two groups based on NAD binding to diphtheria toxin (DT) and cholera toxin (CT).[21,22] The DT group of toxins modifies eukaryotic elongation factor 2 and disrupts protein synthesis in eukaryotic cells. Members of this group include DT, exotoxin A (ETA), and cholix toxin. The CT group of toxins targets various essential proteins within host organisms. For example, CT and heat-labile enterotoxin target Arg on the $G_{s\text{-}\alpha}$ of the G protein, causing uncontrolled adenylate cyclase stimulation; pertussis toxin targets Cys on G_i and uncouples G proteins from the adenylate cyclase pathway; C3bot1 exoenzyme targets Asn41 on Rho A, B, C and result in disaggregation of actin cytoskeleton; vegetative insecticidal protein 2 (VIP2) and iota toxins target Arg177 on actin and prevent actin polymerization.[21,22] Thus, ADPRTs serve as drug targets for treating infections by these lethal bacteria.[23−29]

Although PARP and ADPRT enzymes exhibit diverse functions and low sequence identity,[2,22] they share some common structural and functional features. First, they catalyze a common reaction, namely, ADP-ribosylation whereby

*To whom correspondence should be addressed. Phone: 886-2-2652-3031. Fax: 886-2-2788-7641. E-mail: carmay@gate.sinica.edu.tw.

[a] Abbreviations: 3AB, 3-aminobenzoic acid; ADPRT, ADP-ribosylating toxin; CT, cholera toxin; C3bot1, C3bot1 exoenzyme; C3stau2, C3 exoenzymes from *S. aureus*; DT, diphtheria toxin; ETA, exotoxin A; Ecto-ART2, ecto-ADP-ribosyl transferase 2.2; MD, molecular dynamics; NAD, nicotinamide adenine dinucleotide; 4ANI, 4-amino-1,8-naphthalimide; NMN, nicotinamide mononucleotide; PARP, poly ADP-ribose polymerase; rmsd, root-mean-square deviation; VIP2, Vegetative insecticidal protein 2; vdW, van der Waals.

 Published on Web 04/26/2010 © 2010 American Chemical Society

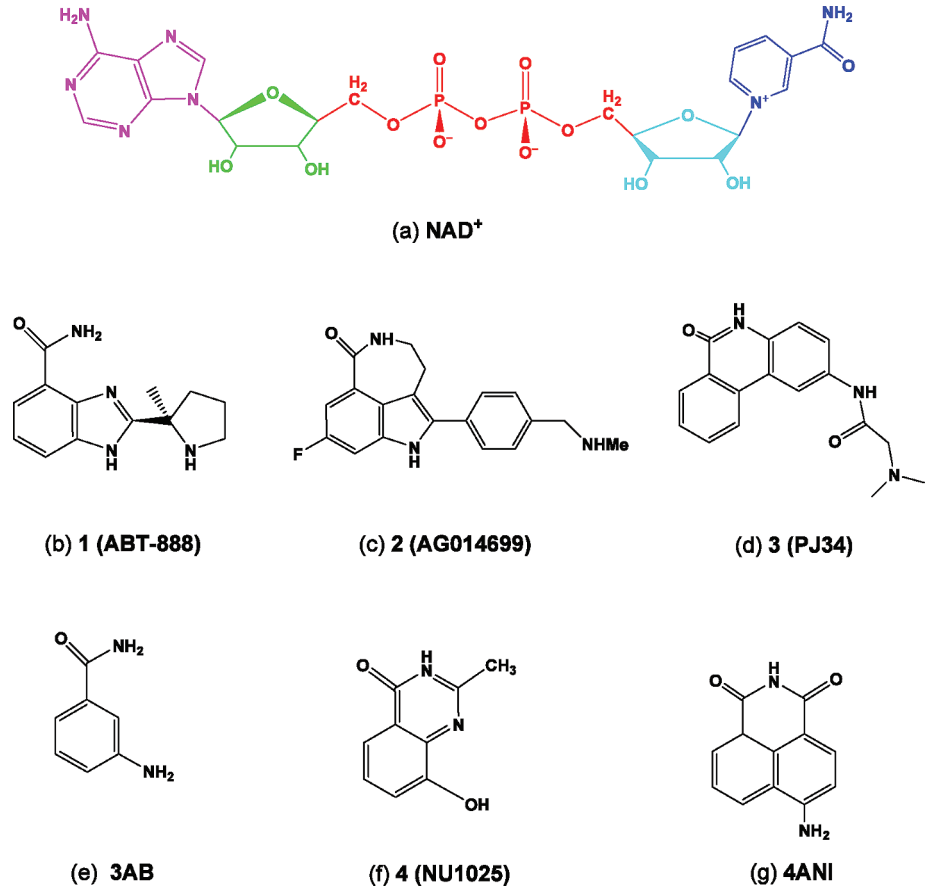

Figure 1. Schematic diagram showing (a) NAD^+, (b) **1**, (c) **2**, (d) **3**, (e) 3AB, (f) **4**, and (g) 4ANI. The NAD^+ diagram was adapted from Yates et al.[33] with the nicotinamide in blue, *N*-ribose in turquoise, diphosphate in red, *N*-ribose in green, and adenine in magenta. The net charge is −1 for NAD^+ and −2 for NADH.

Scheme 1. Common Reaction Catalyzed by PARP and ADPRT Enzymes

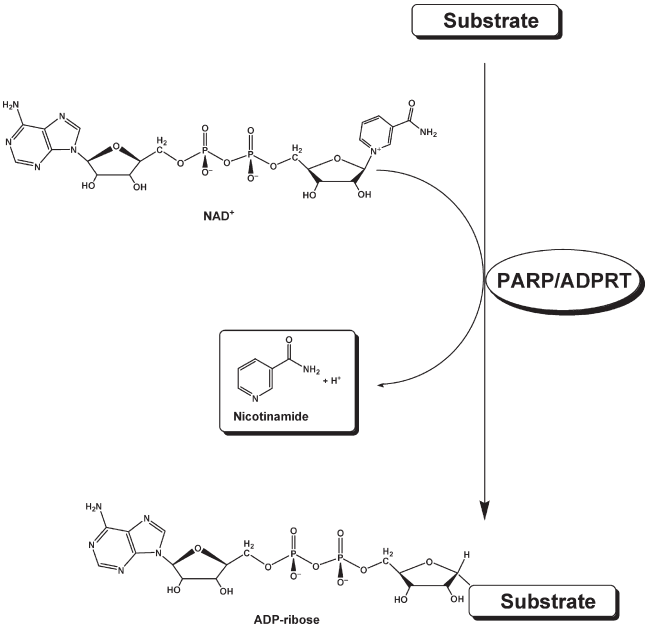

the C−N bond between nicotinamide and the *N*-ribose of NAD^+ is cleaved and the ADP-ribose moiety is subsequently transferred to their targets (Scheme 1). Second, they possess structurally similar catalytic domains; the 3D structures including the NAD^+-binding residues can be well superimposed in DT, ETA, PARP-1, and PARP-2.[3,30] Third, they share common inhibitors such as **3** (PJ34,[31] Figure 1d), which mimics the structure of the NAD^+ nicotinamide and provides a template for the design of new inhibitors.[20,30,32,33]

How do the ADPRTs and PARPs recognize the common substrate NAD^+? In the CT group of toxins, the STS (Ser-Thr-Ser) motif is known to play an important structural role in stabilizing and maintaining the active site conformation, as well as a catalytic role in cleaving NAD^+.[21,34] In C3bot1, Ecto-ART2 (ecto-ADP-ribosyl transferase 2.2 from rat), C3Stau2 (C3 exoenzymes from *S. aureus*), and VIP2, the first Ser of the STS motif hydrogen bonds to the catalytic invariant glutamate to hold it in the correct orientation to catalyze the NAD cleavage.[21,35] The Thr of the STS motif forms hydrogen bonds with perpendicular β-strands to stiffen the active site, while the second Ser in C3bot1 makes hydrogen bonds with the loop immediately following the STS residues forming the β-sheet (see Figure 2).[21] In the DT group of toxins and the PARP family, the STS motif is replaced by the $Y-X_{10}-Y$ motif where the two conserved Tyr contribute $\pi-\pi$ interactions with the nicotinamide ring.[21,29,30,33] The aromatic stacking is thought to (i) expose the anomeric ribose carbon for nucleophilic attack and (ii) orient NAD^+ in an optimal position for interaction with the catalytic Glu. Thus, the $Y-X_{10}-Y$ motif in DT and ETA may bind NAD^+ in a specific conformation. It is not clear, however, if the NAD^+ conformation in DT/ETA differs from that in the CT group of

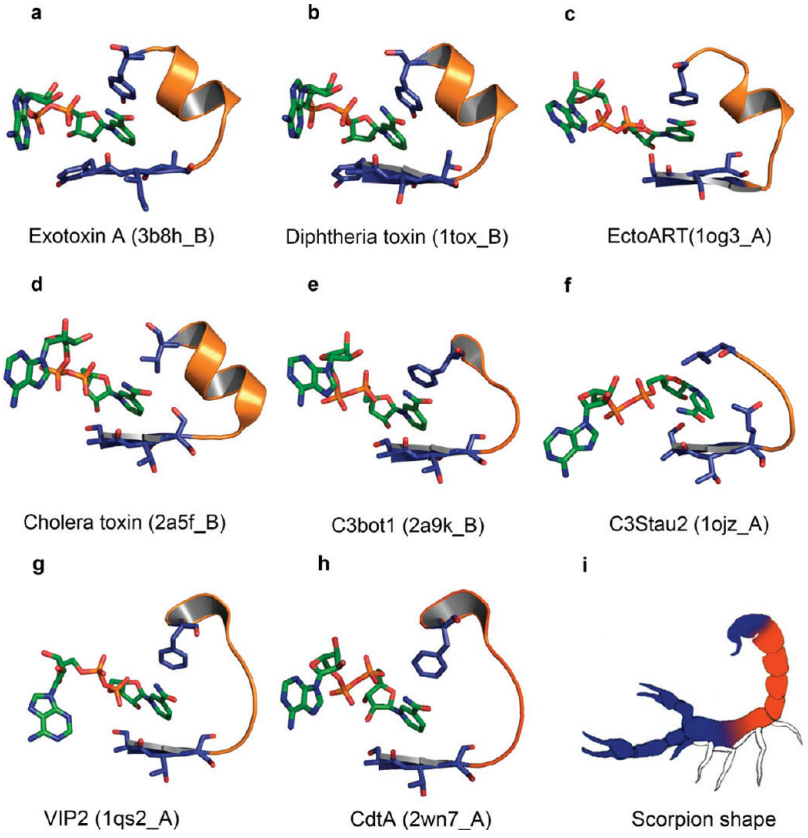

Figure 2. Locally conserved NAD^+-binding site structure in (a) exotoxin A (3b8h_B), (b) diphtheria toxin (1tox_B), (c) EctoART(1og3_A), (d) cholera toxin (2a5f_B), (e) C3bot1 (2a9k_B), (f) C3Stau2 (1ojz_A), (g) VIP2 (1qs2_A), (h) CdtA (2wn7_A), and (i) scorpion shape. The first three residues and the last residue comprising the scorpion motif, which dictate the interactions with NAD^+, are in blue. The NAD atoms are colored green for carbon, blue for nitrogen, red for oxygen, and orange for phosphorus. The secondary structure analysis is according to the STRIDE Web site (http://webclu.bio.wzw.tum.de/cgi-bin/stride/stridecgi.py). The figures were prepared using PyMOL (http://www.pymol.org).

toxins, which employ the STS motif instead of the $Y-X_{10}-Y$ motif to recognize NAD^+.

Despite the aforementioned studies, several intriguing questions remain: (1) Do the $Y-X_{10}-Y$ and STS motifs share any structural similarity in X-ray structures complexed with NAD^+? (2) If so, which forces, electrostatic or van der Waals (vdW), and residues contribute most to binding NAD^+? (3) If the ADPRT and PARP enzymes do share a locally conserved structure for binding NAD^+, do they recognize the same or different NAD^+ conformations? (4) What would be the biological implications/applications of such a structural motif? These questions are addressed in this work. The X-ray structures of toxins/PARPs complexed with NAD^+ reveal that the $Y-X_{10}-Y$ and STS motifs share a locally conserved structure for binding the nicotinamide ring of NAD^+. On the basis of these results, a simple method to precisely dock inhibitor candidates into the ADPRTs and PARPs was proposed. Since docking and quantitative structure−activity relationship analyses have been used to design potent and selective PARP inhibitors,[19,36] our results appear timely in aiding the structure-based design of PARP inhibitors.

Results

Locally Conserved Structure for Binding NAD^+. The "Scorpion" Motif. To determine if the $Y-X_{10}-Y$ motif in the DT group of toxins and the STS motif in the CT group of toxins share any structural similarity, we examined the NAD-bound structures of these two groups of toxins reported in previous work.[21,22] These include DT (1tox) and ETA (3b8h) in the DT group, as well as ectoART (1og3), CT (2a5f), iota (1giq), C3Stau2 (1ojz), VIP2 (1qs2), C3bot1 (2a9k), salmonella virulence protein SpvB (2gwl), and CdtA (2wn7) in the CT group (Table 1). Since the inhibitor, **3** (Figure 1d), is found to bind in the NAD^+-binding site in ETA, we also examined all PDB structures of toxins and PARPs bound to **3** or other inhibitors. For PARPS with multiple structures of bound inhibitors, the structure with an inhibitor that has completed phase II trials (e.g., **1**) was chosen. All the PARP and toxin sequences in Table 1 share ≤36% sequence identity with one another except for two related pairs; PARP-14 and PARP-15 share ~65% sequence identity, while CdtA and Iota toxins share ~86% sequence identity. Although most of the NAD^+/inhibitor-bound toxins share insignificant overall sequence identity, they exhibit a surprisingly structurally conserved NAD^+/inhibitor-binding site, as shown in Figure 2 for the NAD^+-bound structures and in Supporting Information Figure S1 for the other structures in Table 1. This locally conserved structure is shaped like a scorpion ready to sting its prey, the NAD^+ nicotinamide ring or the inhibitor's aromatic ring; hence, it is termed the "scorpion" motif. The scorpion's head is a Tyr or Ser, while its tail consists of a highly conserved aromatic residue (Tyr, Phe, or Trp) or an aliphatic residue (Val or Leu) above the NAD^+ nicotinamide ring (Table 1). The other residues comprising the scorpion motif appear to be more variable than the first and last residues.

Table 1. Scorpion Motifs in X-ray Structures of PARPs/Toxins Complexed with NAD Substrate or Inhibitor

				scorpion motif		
PDBid_Chain	resolution (Å)	toxin/PARP	ligand[a]	sequence[b]	length[c]	rmsd[d] (Å)
				Type I		
1. 1og3_A	2.60	EctoART	NAD^+	^{147}SSSL**SKKVAQ**SQEF^{160}	14	0.69
2. 1tox_B	2.30	DT	NAD^+	^{54}YSTDN**KYDAAG**Y^{65}	12	0.57
3. 1xk9_A	2.10	ETA	**3**	^{470}YIAGD**PALAYG**Y^{481}	12	0.27
4. 2a5f_B	2.02	cholera	NAD^+	^{61}STSI**SLRSAH**LV^{72}	12	1.01
5. 2pqf_F	2.20	PARP-12	3AB	^{596}YFARD**AAYSHH**Y^{607}	12	0.56
6. 2q6m_A	1.25	cholix	**3**	^{493}YVATH**AEVAHG**Y^{504}	12	0
7. 2rd6_A[e]	2.30	PARP-1	**1**	^{235}YFADM**VSKSAN**Y^{246}	12	0.33
8. 3b8h_B	2.50	ETA	NAD^+	^{470}YIAGD**PALAYG**Y^{481}	12	0.26
9. 3ce0_A	2.80	PARP-3	**3**	^{414}YFASE**NSKSAG**Y^{425}	12	0.29
10. 3gey_A	2.20	PARP-15	**3**	^{569}YFAVD**ASYSA**KDTY^{582}	14	0.66
11. 3goy_A	2.80	PARP-14	3AB	^{1633}YFAVN**ANYSA**NDTY^{1646}	14	0.74
12. 3hkv_A	2.10	PARP-10	3AB	^{919}YFAKR**ASLSV**QDRY^{932}	14	0.67
13. 3kjd_A	1.95	PARP-2	**1**	^{462}YFADM**SSKSAN**Y^{473}	12	0.40
				Type II		
14. 1giq_A	1.80	iota	NADH	^{338}STSIGSVNMSAF^{349}	12	3.26
15. 1ojz_A	2.02	C3Stau2	NAD^+	^{138}STQLVSGAAL^{147}	10	1.41
16. 1qs2_A	2.70	VIP2	NAD^+	^{386}STSLSSERLAAF^{397}	12	3.16
17. 2a9k_B	1.73	C3bot1	NAD^+	^{174}STSLMNVSQF^{183}	10	1.10
18. 2gwl_A	1.90	SpvB	NADH	^{501}STSPDKAW^{508}	8	1.39
19. 2wn7_A	2.25	CdtA	NAD^+	^{345}STSIGSVNM**SAF**^{356}	12	3.21

[a] The ligands are illustrated in Figure 1. [b] Underlined residues are located in a β-strand, and bold residues are part of an α-helix. The remaining scorpion residues are located in turn/loop regions. The sequence numbering and secondary structures assignment are according to the respective PDB entries. [c] The number of residues comprising the scorpion motif. [d] Root-mean-square deviation of the C^α backbone atoms of the scorpion motif in a given toxin from those in the cholix toxin. [e] The sequence numbering in 2rd6_A corresponds to ^{896}YFADM**VSKSANY**^{907} in other studies.[20]

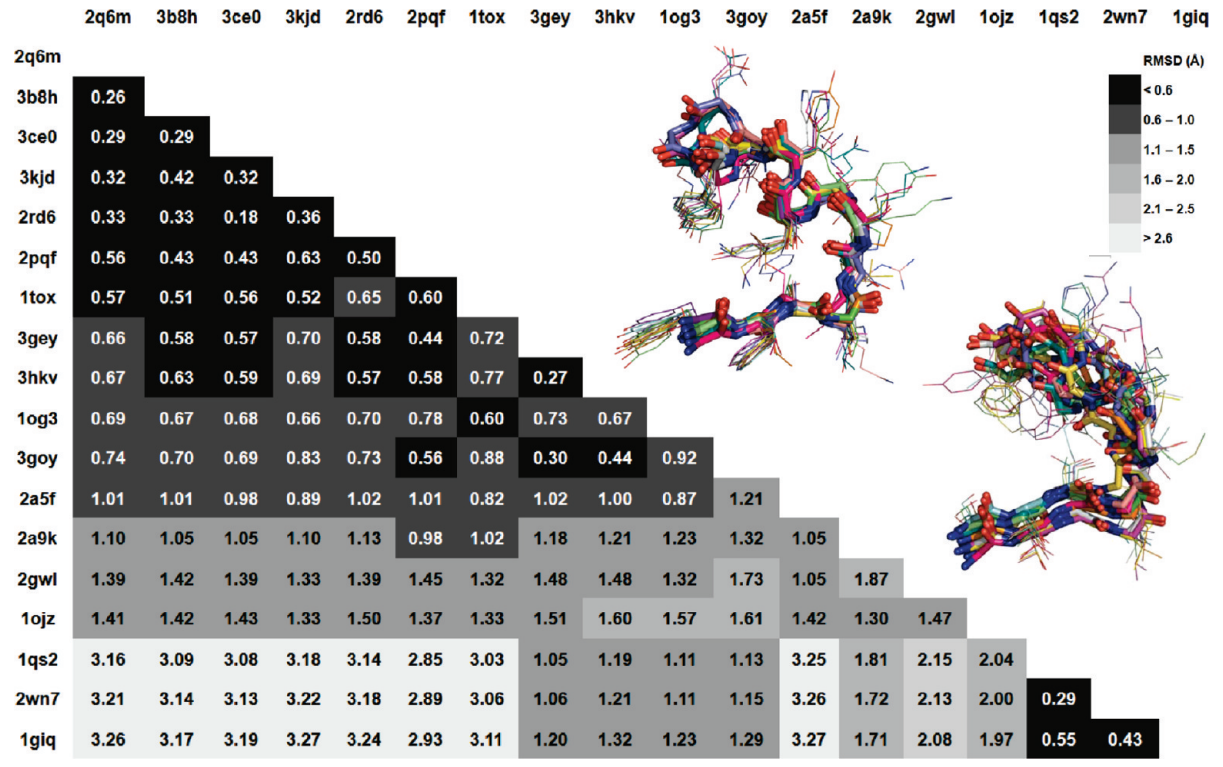

Figure 3. Pairwise C^α rmsd in Å of the scorpion motifs in Table 1, computed as described in the Materials and Methods section. These are ranked in order of increasing rmsd relative to the 2q6m structure. Overlap of the C^α backbone of type I/II scorpion motifs in Table 1 is shown in the upper triangle.

Scorpion Motif Isotypes. To assess the similarity of the scorpion motif structures, the root-mean-square-deviation values (rmsd values) of the C^α atoms for each pair of scorpion motifs in Table 1 were computed. The values in Figure 3 show two groups of scorpion motifs. The first group of scorpion motifs comprises 11 $Y-X_{10-12}-Y$ motifs (1tox, 1xk9, 2pqf, 2q6m, 2rd6, 3b8h, 3ce0, 3gey, 3hkv, 3goy, and 3kjd) and 2 STS motifs (1og3 and 2a5f) with pairwise rmsd values of ≤ 1 Å, comparable to thermal fluctuations; we will refer to such similar structures as type I scorpion motifs. Their 3D structures complexed with NAD^+ (Figures 2a–d) and inhibitors (Supporting Information Figure S1a–i) share

Table 2. Average Electrostatic (E^{elec}) and vdW (E^{vdW}) Contributions to the Interaction Energy between the Scorpion Residues and NAD^+

protein bound to NAD^+ [a]	E^{vdW} (kcal/mol)	E^{elec} (kcal/mol)
VIP2	-9.0 ± 1.0	11.2 ± 2.7
EctoART	-11.1 ± 1.7	-1.9 ± 10.2
CdtA	-12.7 ± 2.1	2.7 ± 10.2
CT	-13.5 ± 1.2	-2.0 ± 2.9
C3bot1	-15.8 ± 1.4	-0.8 ± 4.5
C3Stau2	-16.2 ± 1.5	-11.8 ± 3.1
ETA	-19.7 ± 1.6	0.4 ± 3.4
DT	-20.0 ± 2.0	13.5 ± 6.0

[a] The PDB entries and corresponding residues comprising the scorpion motif are listed in Table 1. The toxins are listed in order of decreasing E^{vdW}.

in common a structured helical tail that ends usually with an aromatic residue (except in CT; see Table 1). The second group of scorpion motifs comprises six STS motifs (1giq, 1ojz, 1qs2, 2a9k, 2gwl, and 2wn7) with pairwise rmsd values ranging from 1 to 3.3 Å; we will refer to these more variable structures as type II scorpion motifs. Their 3D structures complexed with NAD^+ (Figures 2e−h) or NADH (Supporting Information Figure S1j,k) reveal a STS/Q head and an unstructured tail. Interestingly, iota (1giq), CdtA (2wn7), and VIP2 (1qs2), which target the same residue (Arg177) on actin,[21,22] possess very similar scorpion conformations with pairwise rmsd values of ≤0.55 Å.

vdW Forces Dictate the NAD^+ Recognition by the Scorpion Motif. To provide a physical basis for the structural conservation of the "scorpion" motif in binding NAD^+, the electrostatic (E^{elec}) and vdW (E^{vdW}) contributions to the total interaction energy between the residues comprising the scorpion motif (scorpion residues) and NAD^+ were computed from MD simulations of the toxin/NAD^+ complexes in Table 1 (see Materials and Methods). The magnitude and sign of E^{elec} and E^{vdW} in Table 2 show that the scorpion motif recognizes NAD^+ mainly via vdW forces. The E^{vdW} energies are consistently favorable (negative) for the toxins in the DT and CT families. Furthermore, they are more favorable than the corresponding E^{elec} energies (which are usually negligible or unfavorable) with standard deviations less than those of E^{elec}.

Electrostatic Contributions from Nicotinamide and Diphosphate Cancel. To determine why E^{elec} is less favorable than E^{vdW}, the E^{elec} and E^{vdW} energies between each scorpion residue and NAD^+ (Figure 4, black curves with circles) were decomposed into the contributions from nicotinamide (blue), *N*-ribose (turquoise), diphosphate (red), A-ribose (green), and adenine (magenta) for all the NAD^+-bound toxins. The E^{elec} and E^{vdW} energies for NAD^+-bound DT, ETA, CT, and VIP2 are shown in Figure 4, while those for the other NAD^+-bound toxins are shown in Supporting Information Figure S2. The E^{elec} between each scorpion residue and NAD^+ (Figure 4 and Supporting Information Figure S2, top panels) show that the charged residues exhibit large $|E^{elec}|$, but their interactions with the positively charged nicotinamide moiety (blue curves) roughly cancel those with the negatively charged diphosphate (red curves) so that the net E^{elec} contribution (black curves with circles) is generally negligible or unfavorable. In ETA for example, the only charged residue comprising the scorpion motif, D474, contributes a favorable E^{elec} of about −20 kcal/mol with the positively charged nicotinamide but an equally unfavorable E^{elec} of ∼20 kcal/mol with the doubly negatively charged diphosphate, so the net E^{elec} between the scorpion residues and NAD^+ is negligible (0.4 kcal/mol).

The Scorpion Head and Tail Contribute Most to Binding NAD^+. The E^{vdW} between each scorpion residue and NAD^+ (Figure 4 and Supporting Information Figure S2, bottom panels) show that the vdW contributions of the first three and last scorpion residues are greater than those of the other scorpion residues, consistent with their relative conservation and distances to NAD^+. In the DT group represented by DT (Figure 4a) and ETA (Figure 4b), the first and last residues of the scorpion motif, which are both Tyr, contribute much more to binding NAD^+ than the other residues. These two tyrosines correspond to the conserved Tyr in the $Y-X_{10}-Y$ sequence motif. In the CT group represented by CT (Figure 4c) and VIP2 (Figure 4d), as well as EctoART, C3Stau2, C3bot1, and CdtA (Supporting Information Figure S2), the first three and last residues of the scorpion motif contribute more to binding NAD^+ than the other residues. The first three residues comprising the scorpion head in the CT toxins correspond to the STS motif, which forms part of the β-sheet that acts as an anchor to hold the NAD^+.[34] In CT toxins such as CT and C3Stau2 where the scorpion tail is an aliphatic residue, the scorpion STS/Q head apparently makes a larger vdW contribution than the respective aliphatic tail.

The Scorpion Motif Recognizes the NAD^+ Nicotinamide Ring. The results in Figure 4 show that the scorpion motif is primarily a nicotinamide-binding motif: The vdW interaction energies of the scorpion residues with nicotinamide (blue curves) are significantly more favorable than those with the ribose rings (green or turquoise curves), the diphosphate (red curves), or adenine (magenta curves). Moreover, the interaction energies of the scorpion head and tail with NAD^+ stem mainly from those with nicotinamide and, to a lesser extent, with the diphosphate and *N*-ribose. Notably, the adenine mononucleotide portion of NAD makes a negligible contribution to the net interaction energy with scorpion residues. These results are consistent with the respective structures depicted in Figure 2.

The Scorpion Motif Binds NMN in a Specific Conformation. Since the scorpion motif is structurally conserved and is involved in binding the NAD^+ nicotinamide ring, is the conformation of the nicotinamide mononucleotide (NMN) moiety also conserved? To address this question, the NMN moieties of the eight NAD^+ molecules in Table 1 were superimposed. The eight NAD^+ conformations in Figure 5 show that both types I and II scorpion motifs bind the NMN moiety in a structurally conserved ringlike conformation stabilized by a hydrogen bond between the nicotinamide amide nitrogen and the *N*-phosphate oxygen. In sharp contrast, the adenine mononucleotide structures exhibit highly variable conformations even when their moieties, instead of NMN, were superimposed (data not shown). The different structural conservation of the NMN and adenine mononucleotide moieties of NAD are consistent with their different relative contributions to the net interaction energy with the scorpion residues. Previous work has also noted that iota toxin binds NADH in a specific NMN ringlike conformation, whereby the "ring" is closed by a hydrogen bond between the nicotinamide carboxyamide nitrogen and a phosphate oxygen.[37]

The Scorpion Motifs Can Serve as Templates for Predicting Bound Inhibitor Structure. Since proteins with the type I scorpion motif possess very similar structures, we propose a "docking by fitting" method to precisely dock an inhibitor mimicking the nicotinamide ring into ADPRTs and PARPs

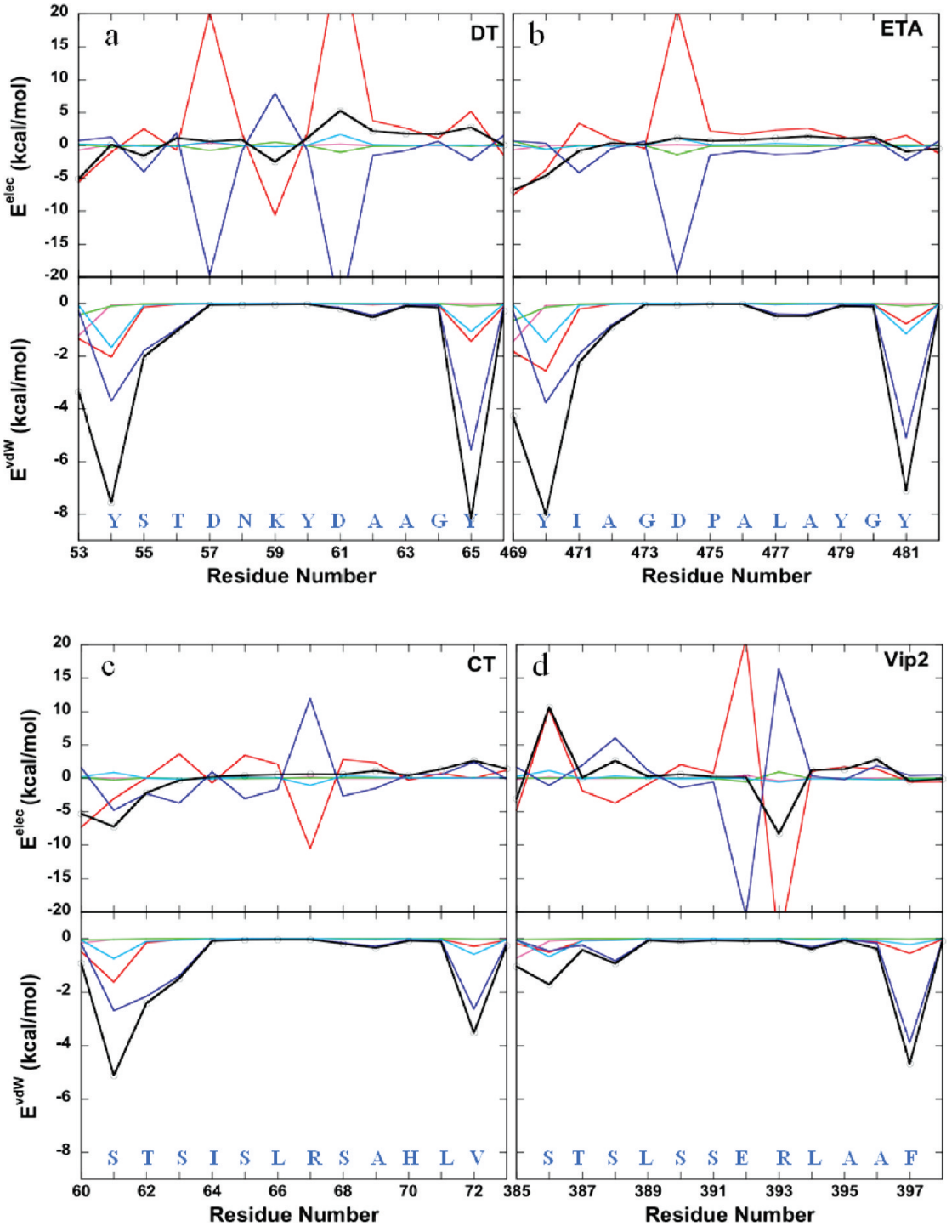

Figure 4. Electrostatic (E^{elec}) and vdW (E^{vdW}) interaction energies (in kcal/mol) of the scorpion residues with NAD^+ (black), nicotinamide (blue), *N*-ribose (turquoise), diphosphate (red), *N*-ribose (green), and adenine (magenta) in (a) DT, (b) ETA, (c) CT, and (d) VIP2.

with free 3D structures. The method is illustrated in Figure 6a, and the predicted structure of PARP-2 bound to **1** is validated against the respective X-ray structure (3kjd) in Figure 6b and Figure 6c. First, the scorpion motifs in the X-ray structures of apoPARP-2 (1gs0) and PARP-1 bound to **1** (2rd6) were superimposed. Next, the PARP-1 structure was removed leaving PARP-2 bound to **1**. Comparison of this docked inhibitor structure (in green) with the X-ray structure of PARP-2 bound to **1** (in blue) in Figure 6b shows almost perfect overlap. Since the pocket is very narrow and deeply buried (see Figure 6c), current docking methods using a scoring function may yield a false-positive inhibitor-binding site without empirical restraints to guide docking of the inhibitor into this narrow and buried site. However, conventional docking or optimization methods could be used to refine the structure derived using "docking by fitting".

Predicted Scorpion Motifs in PARP and ADPRT Enzymes. Multiple sequence alignment of the catalytic cores of the human PARPs show a conserved Tyr corresponding to the first Tyr of the $Y-X_{10}-Y$ motif. On the other hand, structure-based multiple sequence alignment of the catalytic

cores of 31 mono-ADPRTs[21,22] show the STS motif for 28 toxins in the CT group and the Y−X_{10}−Y motif for DT, ETA, and cholix. The analyses of the available X-ray structures of toxins complexed with NAD^+ herein show that the head and tail residues of the scorpion motif contribute most to binding NAD^+ and are relatively conserved. The "scorpion's" head is a Tyr or Ser, while its tail is a highly conserved aromatic or aliphatic residue (Table 1). For the PARPs/toxins whose 3D structures with substrate/inhibitor have *not* been solved, putative scorpion sequences were obtained by searching for an aromatic residue (Y, F, W, H) or an aliphatic residue (L, I, V, A) at ≤15 residues from (i) the conserved Tyr in PARPs or (ii) the conserved Ser in the CT group of toxins. For those PARPs/toxins whose free (but not complex) 3D structures are available, the putative scorpion motifs were verified by computing the rmsd values of their C^α atoms from the C^α atoms in the cholix scorpion motif (see Materials and Methods). The resulting rmsd values in Table 3 are all < 2.1 Å, verifying the presence of the scorpion motif in these free protein structures. Notably, the scorpion motif in PARP-5a is of type I with a C^α rmsd of only 0.32 Å and a helical tail (indicated by the bold residues in Table 3). For the PARPs and toxins whose 3D structures have not yet been solved, their scorpion sequences are listed in Table 4. Of the 17 human PARPs, 14 exhibit the Y−X_{10-13}−Y motif, while PARP-7 and PARP-11 have a Phe in lieu of the second Tyr; i.e., they contain a Y−X_{10}−F motif. Only PARP-9 does not seem to have a scorpion motif, as no aromatic residue is found at even 20 residues C-terminal from the conserved Tyr.

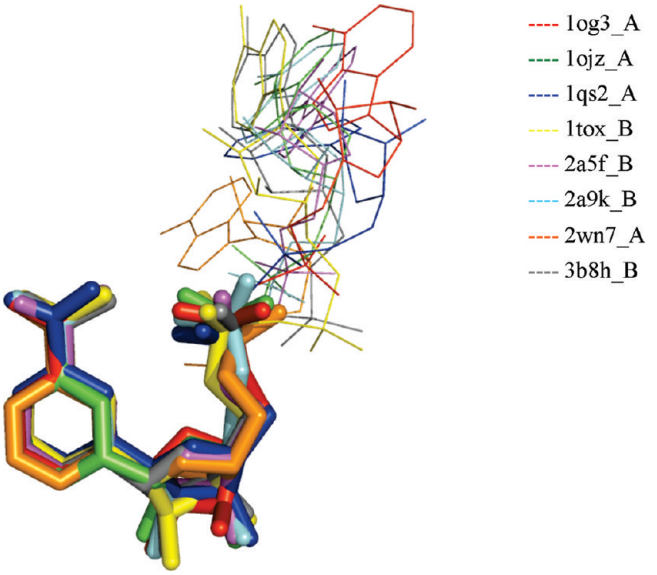

Figure 5. Conformations of the NAD^+ molecules bound to the scorpion motifs in Table 1 by overlapping their NMN moieties.

Discussion

The Scorpion Motif. A Conserved Architecture in PARP and ADPRT Enzymes. This work shows that although PARP and ADPRT enzymes exhibit diverse functions and low sequence identity, they share a common structure shaped like a scorpion to recognize their common substrate (Figure 2). The scorpion motifs can be further divided into two isotypes according to their structural similarity: the type I scorpion motifs have very similar conformations with C^α rmsd values of ≤1 Å (Figure 3), comparable to the differences found in NMR generated ensembles, whereas the type II scorpion motifs possess more variable conformations. On the basis of current X-ray structures, all the PARPs and DT group toxins as well as two CT group toxins (EctoART and CT) exhibit a type I scorpion motif, whereas the other CT group toxins display a type II scorpion motif. Biological applications of the highly conserved type I scorpion motif are described below.

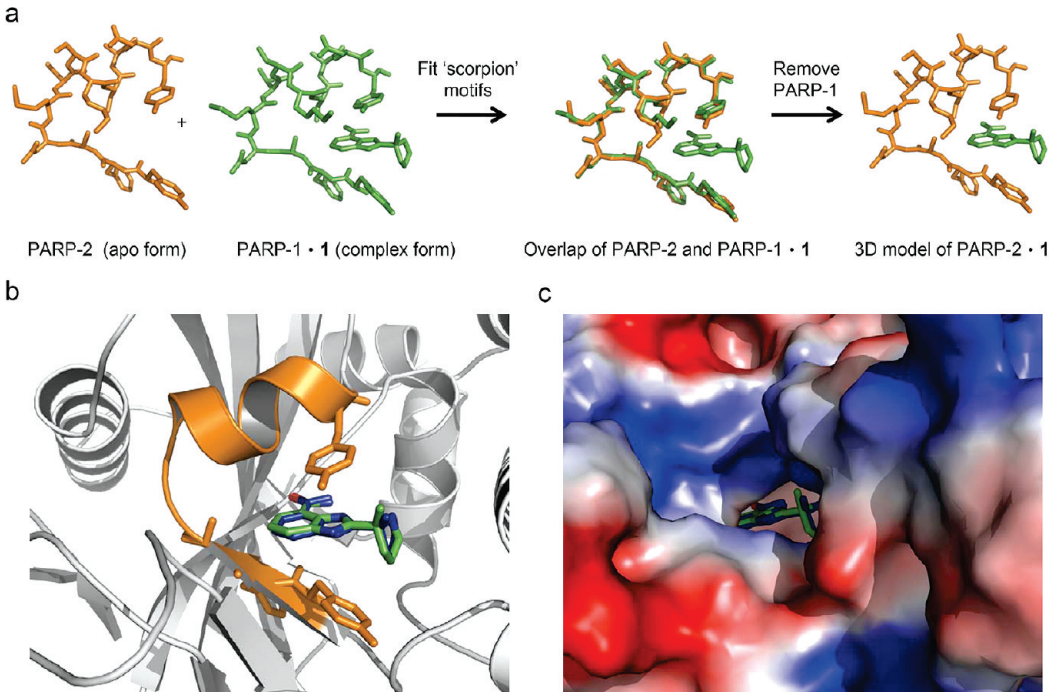

Figure 6. (a) Illustration of docking by fitting the scorpion motifs of apo-PARP-2 (1gs0) and PARP-1 bound to **1** (2rd6). (b) Comparison between the predicted (green) and X-ray (blue) structures of PARP-2 bound to **1**. (c) View showing that inhibitor-binding pocket is very narrow and deeply buried.

Table 3. Predicted Scorpion Motifs in X-ray Structures of Free PARPs/ADPRTs[a]

PDBid_Chain	resolution (Å)	toxin/PARP	scorpion motif		rmsd (Å)
			sequence	length	
2rf5_A	2.30	PARP-5a	^{1213}YFAEN**SSKSNQY**^{1224}	12	0.32
1lts_A	1.95	LT-A	^{61}STSLS**LRSAHLA**^{72}	12	1.06
1tii_A	2.25	LT-IIB	^{59}STTTT**LRQAHLL**^{70}	12	1.16
1bcp_A	2.70	PT	^{52}STSSS**RRYTEVY**^{63}	12	1.25
1r45_A	1.57	C3bot2	^{174}STSLMS**AQF**^{182}	9	1.64
3bw8_A	1.80	C3lim	^{134}STSLVNG**SAF**^{143}	10	1.82
2j3x_A	1.75	C2-I	^{348}STSLKSTP**SSF**^{358}	11	2.07

[a] Entries are listed according to increasing C^{α} rmsd values, which were computed relative to the scorpion motif of cholix toxin (2q6m). See footnotes to Table 1.

Table 4. Putative Scorpion Motifs in ADPRT and PARP Sequences

PARP/toxin	species	UniProt entry	scorpion motif sequence	length
PARP-4	*Homo sapiens*	Q9UKK3	^{477}YFSDSLSTSIKY^{488}	12
PARP-5b/TNKS-2	*Homo sapiens*	Q9H2K2	^{1060}YFAENSSKSNQY^{1071}	12
PARP-6	*Homo sapiens*	Q2NL67	^{508}YLSPISSISFGY^{519}	12
PARP-7	*Homo sapiens*	Q7Z3E1	^{564}YFAKKASYSHNF^{575}	12
PARP-8	*Homo sapiens*	Q8N3A8	^{732}YLSPMSSISFGY^{743}	12
PARP-11	*Homo sapiens*	Q9NR21	^{229}YFARDAAYSSRF^{240}	12
PARP-13	*Homo sapiens*	Q7Z2W4	^{819}YFAKDAIYSHKNCPY^{833}	15
PARP-16	*Homo sapiens*	Q8N5Y8	^{182}YLTSDLSLALIY^{193}	12
ExoS	*P. aeruginosa*	Q51451	^{343}STSLNPGVARSF^{354}	12
AexT	*A. salmonicida*	Q93Q17	^{364}STSRDPKVATNF^{375}	12
ExoT	*P. aeruginosa*	Q9I788	^{346}STSRDPGVARSF^{357}	12
VopT	*V. parahemolyticus*	Q87GI9	^{146}STSRDPEIACEF^{157}	12
Sa	*C. spiroforme*	O06497	^{384}STSIGSVNMSAF^{395}	12
C3cer	*B. cereus*	Q8KNY0	^{142}STSILIDAGY^{151}	10
C3stau1	*S. aureus*	P24121	^{173}STQLVSGAAV^{182}	10
C3stau3	*S. aureus*	Q8VVU2	^{173}STQLVKGAAL^{182}	10
HopU1	*P. syringae*	Q88A91	^{193}STTRIKDSAQVF^{204}	12

Electrostatic vs vdW Forces Underlying NAD^+ Binding. The electrostatic and vdW contributions to the total interaction energy between the scorpion residues and NAD^+ in Table 2 and Figure 4 reveal a fine balance between the electrostatic and vdW forces. An apparent requirement for optimal binding to anionic NAD^+, comprising a positively charged nicotinamide and a doubly negatively charged diphosphate, is to minimize the electrostatic energy of the charged scorpion residues. Most toxins achieve this by positioning the charged scorpion residues and the charged NAD^+ moieties precisely such that the electrostatic interactions of the charged scorpion residues with the dianionic diphosphate effectively cancel those with the cationic nicotinamide while enabling strong vdW interactions with the nicotinamide ring (see Figure 4 and Supporting Information Figure S2). Therefore, mutations that lead to a wrong orientation of the diphosphate relative to the nicotinamide or mutations that alter the charged residue composition of the scorpion motif would be expected to alter the NAD^+ binding affinity and/or the NAD^+-dependent function.

Relationship between the Scorpion Motif and Known Sequence Motifs. This work not only reveals a locally conserved scorpion structure for ADPRT and PARP enzymes but also a locally conserved ringlike NMN structure for the NAD^+ substrate. Since the NMN moiety is conserved but the scorpion motif mainly recognizes only the NMN's nicotinamide ring, this implies that surrounding residues may also contact NMN and that other features of the NAD^+-binding pocket could dictate whether the substrate/inhibitor could fit in the same site. Indeed, the scorpion motif is related to several known sequence motifs and conserved residues that have been identified in PARPs and ADPRTs through multiple sequence alignment, as shown in Figure 7a−c. It corresponds to the known $Y-X_{10}-Y$ motif in the DT group but to a combination of the STS motif (scorpion head) and the N-terminal part of the PN loop (scorpion tail) in the CT group.

The specific NMN conformation recognized by the scorpion motif is held in place by conserved hydrogen-bonding interactions with residues from the other known motifs. Notably, the HG motif in the DT group and RX motif in the CT group are involved in orienting the nicotinamide ring. The conserved Gly of the H**G** motif and the variable residue X of the R**X** motif both form backbone hydrogen bonds with the nicotinamide carboxyamide (Figure 7d and Figure 7e). Furthermore, the invariant catalytic Glu of the ARTT loop hydrogen-bonds with the 2′-OH group of the *N*-ribose with one or both of its carboxylate oxygen atoms in all the NAD^+-bound protein structures. Interestingly, the scorpion motifs in all PARPs (except PARP-9 and PARP-16) contain a Ser at the ninth position whose hydroxyl group also hydrogen-bonds with the amide group in all the inhibitor-bound structures. In summary, the scorpion motif (YY/STS+PN loop) helps to bind the NAD^+ substrate in the narrow nicotinamide-binding crevice, which forces the NMN moiety into a coplanar ringlike conformation; the other known motifs (HG/RX and ARTT loop) then lock this NMN conformation via conserved hydrogen bonds.

Biological Implications. Functional Basis Underlying the Locally Conserved Scorpion Structure. Why do ADPRT and PARP enzymes possess structurally conserved scorpion motifs? One possible reason might be that these enzymes employ a locally conserved scorpion structure to recognize and facilitate the *N*-glycosidic bond cleavage of their common substrate, NAD^+. The scorpion motif recognizes NAD^+ by using its head and tail residues to clasp the

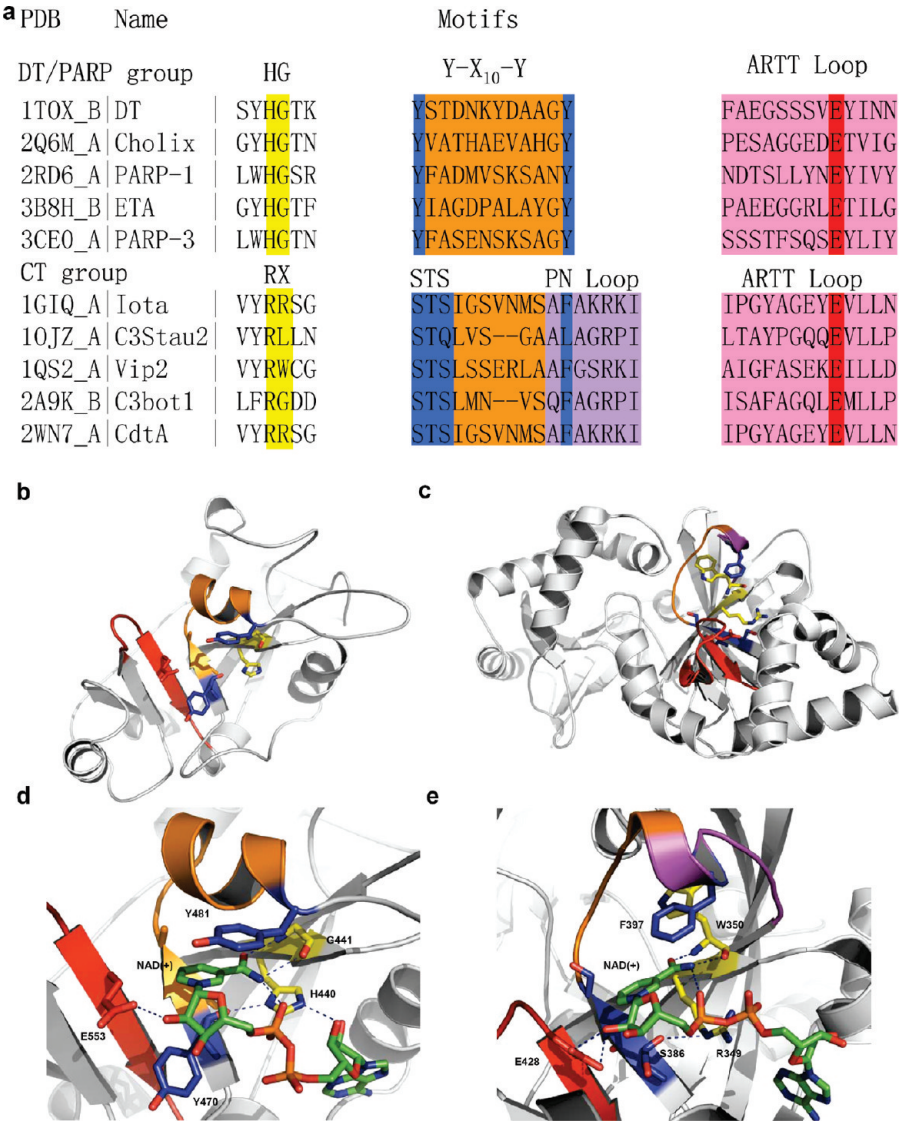

Figure 7. (a) Known motifs from multiple sequence alignment of the ADPRTs and PARPs. The invariant or highly conserved residues in the known motifs are highlighted in different colors. They are shown in the same color scheme in ribbon diagrams of (b) NAD^+-bound ETA (3b8h) and (c) NAD^+-bound VIP2 (1qs2). They form conserved hydrogen bonds, as depicted in the NAD^+-binding sites of (d) ETA (3b8h) and (e) VIP2 (1qs2). The NAD atoms are colored green for carbon, blue for nitrogen, red for oxygen, and orange for phosphorus.

nicotinamide ring by vdW interactions (Figure 4). It also forces the nicotinamide ring to adopt a specific conformation that enables the nicotinamide amide group to anchor the backbone of specific residues. For example, the amide O and N atoms of the nicotinamide ring form two hydrogen bonds with the backbone NH and O of G441 in ETA (Figure 7d) and W350 in VIP2 (Figure 7e). Furthermore, the scorpion motif may bind the nicotinamide ring in a conformation that (i) facilitates cleavage of the C−N bond between the nicotinamide and the *N*-ribose of NAD^+ or (ii) orients the carbon atom for nucleophilic attack.[38]

Biological Applications. Proteins with Locally Conserved Scorpion Structures Can Share Common Inhibitors. Both ADPRTs and PARPs are targets for inhibitor design: inhibition of deadly toxins can rescue the function of their human target proteins, whereas inhibition of PARPs can enhance the effects of anticancer therapies (see Introduction). As the scorpion motif forms the nicotinamide-binding pocket of ADPRTs and PARPs, it can serve as a common drug target for both PARPs and ADPRTs. We hypothesize that those proteins containing highly conserved type I scorpion structures can share common inhibitors mimicking the nicotinamide structure. Indeed, inhibitors such as **3** and 4-amino-1,8-naphthalimide (4ANI, Figure 1g) can inhibit both PARPs and ETA, although their potency to inhibit different ADP-ribosyltransferase family members varies.[20,30,32,33,39] Furthermore, 3-aminobenzoic acid (3AB, Figure 1e) can inhibit not only PARPs but also CT.[40] On the other hand, selective inhibitors for a specific PARP can be designed without inhibiting the other PARPs by optimizing the interactions of the unique residues comprising or surrounding the scorpion motif.

The Scorpion Motif Can Be Used To Predict Inhibitor/Substrate-Bound Structures. Since ADP-ribosylating enzymes containing type I scorpion motifs, which include five ADPRTs (ectoART, DT, ETA, CT, cholix toxin) and eight PARPs (PARP-1, PARP-2, PARP-3, PARP-5a, PARP-10, PARP-12, PARP-14, PARP-15), may share common inhibitors such as **3**, 4ANI, 3AB, and their derivatives, we may predict complex structures of their common inhibitors/substrate using the "docking by fitting" method, illustrated in Figure 6. Notably, the new

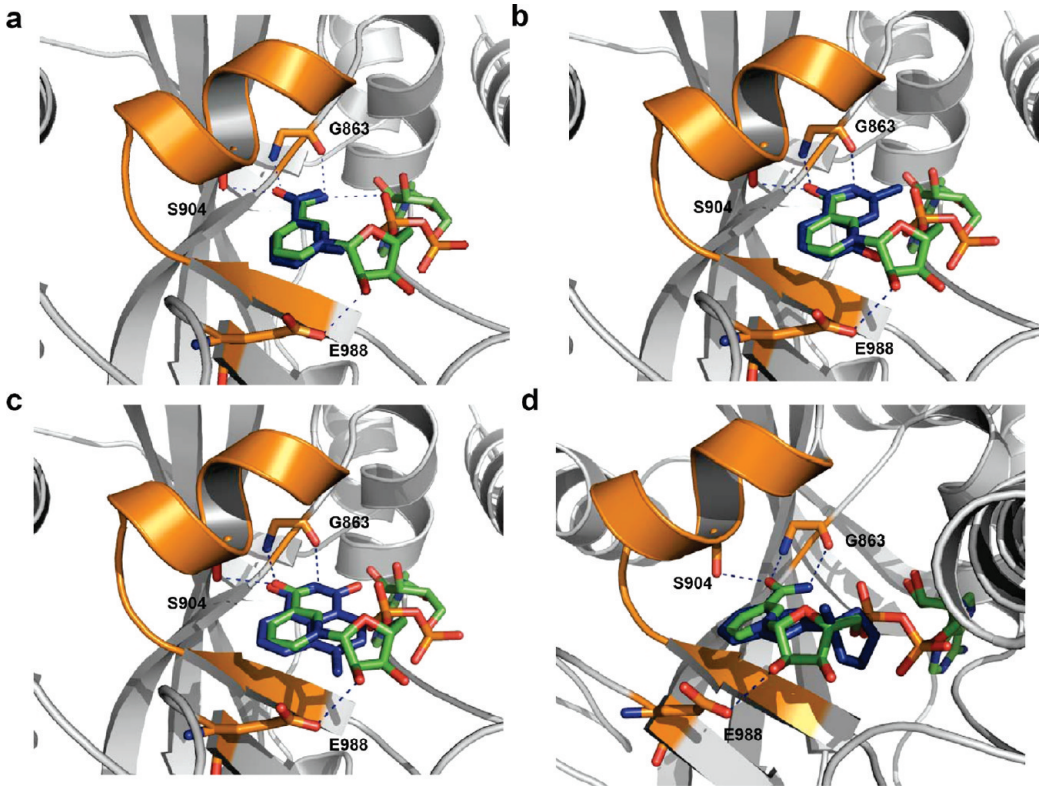

Figure 8. X-ray structures of (a) chicken PARP-1 bound to 3AB (3kcz) and of human PARP-1 bound to (b) **4** (4pax), (c) 4ANI (2pax), and (d) **1** (2rd6). The 3D structure of NAD^+ bound to PARP-1 in (a) was predicted using "docking by fitting" (see text). The PARP-1 scorpion motif is in orange. The inhibitors are in dark blue, while the NAD atoms are colored green for carbon, blue for nitrogen, red for oxygen, and orange for phosphorus.

PARP inhibitors such as **1**, **2**, and olaparib have completed phase II clinical trials for cancer indications.[13] Initial model structures of PARPs complexed with inhibitors/substrate can be derived using "docking by fitting". As shown in Figure 6, the predicted structure of **1** bound to PARP-2 is in good agreement with the respective X-ray structure (3kjd). As another example, model 3D structures of PARP-1 complexed with 3AB (Figure 1e) and NAD^+ substrate (Figure 1a) were obtained by fitting the C^α atoms of the 12-residue scorpion motif in the free PARP-1 structure (2paw) with those in the 3AB-bound PARP-2 (3kcz) and NAD^+-bound ETA (3b8h) structures, respectively. The predicted structures of the 3AB inhibitor and NAD^+ substrate bound to PARP-1 in Figure 8a appear reasonable; they maintained the hydrogen-bonding interactions between the inhibitor/substrate aromatic ring and PARP-1 as well as the critical $\pi-\pi$ interactions with the scorpion tail. Notably, the inhibitor's aromatic ring overlaps with the NAD^+'s nicotinamide ring.

In summary, "docking by fitting" together with conventional docking or optimization methods offers a fast and accurate docking strategy: the former can quickly dock an inhibitor/NAD^+ into the very narrow and deeply buried NAD^+-binding pocket (Figure 6c), while the latter can be used to refine the complex structure, which can serve as a starting point for the structure-based design of ADPRT and PARP inhibitors with improved affinity and selectivity.

Potent Inhibitors Have Stronger Interactions with Residues Comprising and Surrounding the Scorpion Motif. Early PARP inhibitors were based on the benzamide pharmacophore, which mimics the NAD^+ nicotinamide ring: their amide group interacts with the protein backbone atoms, while their aromatic ring interacts with the "scorpion's" head and tail residues (see above). Since they lacked specificity and potency, subsequent inhibitor designs sought to lock the carboxyamide in the favored conformation (i) by incorporating it into a ring system to form a bicyclic ring inhibitor, e.g., **4** (NU1025,[41] Figure 1f) or (ii) through intramolecular hydrogen bonds.[42] However, these inhibitors still needed micromolar concentration for inhibition. Hence, new PARP inhibitors were designed by cyclizing an open benzamide structure or creating an additional ring on the existing cyclic amide to form coplanar bicyclic or tricyclic amide inhibitors (Figures 1b–d), which inhibit PARPs better than monocyclic amide inhibitors such as 3AB and its derivatives.[19] For example, the IC_{50} value of **1** (0.041 μM) is 1–3 orders of magnitude less than that of 4ANI (0.18 μM), **4** (0.40 μM), and 3AB (33 μM).[43,44] To provide a rationale for the observed enhanced inhibition, the scorpion motifs of inhibitor-bound PARP-1 in Figure 8 and NAD^+-bound ETA were superimposed to compare the inhibitor and substrate structures. Interestingly, the [5,6] bicyclic ring of **1** in the 2rd6 structure superposed well with the nicotinamide ring and part of the *N*-ribose, while its five-membered ring is oriented toward the *N*-phosphate group. As shown in Figure 8d, inhibitor **1** resembles the ringlike structure of NMN more than the other inhibitors, 3AB (Figure 8a), **4** (Figure 8b), and 4ANI (Figure 8c), which superposed with only the nicotinamide ring but not with the other parts of NAD^+. The three less potent inhibitors likely fit less tightly than inhibitor **1**, allowing room for water molecules in the NAD^+-binding site, thus attenuating the protein–inhibitor

interaction energies. Indeed, the binding free energies of 3AB, **4**, 4ANI, and **1** to PARP-1 computed using the DFIRE program[45,46] (see Supporting Information Table S1) correlate with $-RT\ln(IC_{50})$, as evidenced by a Pearson correlation coefficient of $r^2 = 0.82$. The binding energies of these four inhibitors to only the scorpion motif also correlate with $-RT\ln(IC_{50})$ with $r^2 = 0.78$. This suggests that the observed enhanced inhibition of inhibitor **1** is due largely to its stronger interactions with the residues comprising and surrounding the scorpion motif (see Figure 7), as compared to the other less potent inhibitors.

Materials and Methods

rmsd Calculations. The number of residues comprising the scorpion motifs in Table 1 varies from 8 to 14. However, this number should be the same to superpose the backbone of two scorpion motifs. Thus, to fit two scorpion motifs of different lengths, residues have to be neglected in the longer motif. In fitting scorpion motifs of lengths l and $l + n$, all combinations of n residues were left out in the longer motif except for the first three and last residues that are important for binding the nicotinamide ring. The C^{α} rmsd values were computed using Swiss-PdbViewer, version 3.7 (http://spdbv.vital-it.ch/index.html), and the lowest rmsd was chosen.

Molecular Dynamics Simulations. To analyze the binding interactions of bacterial toxins with NAD^+, molecular dynamics (MD) simulations were performed starting from the NAD^+-bound structures in Table 1 using the CHARMM, version 34, program[47] at a mean temperature of 300 K and pH 7. The missing hydrogen atoms in the X-ray structures were built at physiological pH. The aspartates and glutamates were deprotonated, while the lysines and arginines were protonated. The protonation states of the histidines were determined by computing the relative free energies of doubly protonated His or His protonated at $N^{\varepsilon 2}$ relative to His protonated at $N^{\delta 1}$.

Force Field. All simulations employed the all-hydrogen CHARMM27 force field for the protein[48] and NAD^+,[49] the TIP3P[50] water model, and periodic boundary conditions in a truncated octahedron.[51] The nonbonded interactions were truncated at 18 Å using an atom-based force-switching function to smoothly switch off the forces from 14 to 17 Å. The SHAKE algorithm was applied to all the bonds to hydrogen atoms.[52]

Simulation Protocol. Each hydrogen-built structure was energy-minimized and then placed at the center of a truncated octahedral box (of square edge of length 70 Å) containing 5706 TIP3P water molecules that were pre-equilibrated at normal water density (1 g/mL) at 298 K. Water molecules within 2.5 Å of any of the protein heavy atoms were removed. The resulting water molecules were re-equilibrated around the fixed protein/NAD^+ molecule. Before equilibration of the simulation system, the protein side chains were energy-minimized together with the water molecules. All the atoms were then propagated according to Newton's equations of motions using the leapfrog Verlet integrator with a time step of 2 fs. The entire system was equilibrated without any constraints for ~500 ps, followed by a production trajectory of 1 ns where the atomic positions were saved every 0.1 ps for further analyses.

Decomposing the Toxin−NAD^+ Interaction Energy into Contributions from Each Residue. To provide a physical basis for the locally conserved scorpion structure, the electrostatics and vdW interaction energies of each of the scorpion residues with NAD^+ was computed from the saved coordinate sets during the production trajectory. To probe the key NAD site that is recognized by this structural motif, the NAD was divided into five components, as shown in Figure 1; viz., the nicotinamide ring that interacts with the head and tail of the scorpion, the *N*-ribose, the diphosphate, the A-ribose, and the adenine, and the electrostatic and vdW interaction energies between each scorpion residue and each NAD^+ component were computed. The final energies plotted in Figure 4 were averaged over 10^4 configurations from each of the 1 ns simulations.

Acknowledgment. We thank Prof. Yaoqi Zhou for sending us his DFIRE program for protein−ligand interactions. This work was supported by the Human Frontiers Science Program, the Institute of Biomedical Sciences, Academia Sinica and the NSC Contract No. NSC 95-2113-M-001-001.

Supporting Information Available: Figure S1 (chemical structures), Figure S2 (plots of energy vs residue number), and Table S1 (listing the binding free energies). This material is available free of charge via the Internet at http://pubs.acs.org.

References

(1) Till, S.; Diamantara, K.; Ladurner, A. G. PARP: a transferase by any other name. *Nat. Struct. Mol. Biol.* **2008**, *15*, 1243–1244.
(2) Ame, J. C.; Spenlehauer, C.; de Murcia, G. The PARP superfamily. *BioEssays* **2004**, *26*, 882–893.
(3) Otto, H.; Reche, P. A.; Bazan, F.; Dittmar, K.; Haag, F.; Koch-Nolte, F. In silico characterization of the family of PARP-like poly (ADP-ribosyl) transferases (pARTs). *BMC Genomics* **2005**, *6*, 139–161.
(4) Hassa, P. O.; Hottiger, M. O. The diverse biological roles of mammalian PARPS, a small but powerful family of poly-ADP-ribose polymerases. *Front. Biosci.* **2008**, *13*, 3046–3082.
(5) Burkle, A. The most elaborate metabolite of NAD+. *FEBS J.* **2005**, *272*, 4576–4589.
(6) Schreiber, V.; Dantzer, F.; Ame, J. C.; de Murcia, G. Poly (ADP-ribose): novel functions for an old molecule. *Nat. Rev. Mol. Cell Biol.* **2006**, *7*, 517–528.
(7) Virag, L.; Szabo, C. The therapeutic potential of poly (ADP-ribose) polymerase inhibitors. *Pharmacol. Rev.* **2002**, *54*, 375–429.
(8) Eliasson, M. J. L.; Sampei, K.; Mandir, A. S.; Hurn, P. D.; Traystman, R. J.; Bao, J.; Pieper, A.; Wang, Z. Q.; Dawson, T. M.; Snyder, S. H. Poly (ADP-ribose) polymerase gene disruption renders mice resistant to cerebral ischemia. *Nat. Med.* **1997**, *3*, 1089–1095.
(9) Ratnam, K.; Low, J. A. Current development of clinical inhibitors of poly (ADP-ribose) polymerase in oncology. *Clin. Cancer Res.* **2007**, *13*, 1383–1388.
(10) Bryant, H. E.; Schultz, N.; Thomas, H. D.; Parker, K. M.; Flower, D.; Lopez, E.; Kyle, S.; Meuth, M.; Curtin, N. J.; Helleday, T. Specific killing of BRCA2-deficient tumours with inhibitors of poly (ADP-ribose) polymerase. *Nature* **2005**, *434*, 913–917.
(11) Farmer, H.; McCabe, N.; Lord, C. J.; Tutt, A. N. J.; Johnson, D. A.; Richardson, T. B.; Santarosa, M.; Dillon, K. J.; Hickson, I.; Knights, C. Targeting the DNA repair defect in BRCA mutant cells as a therapeutic strategy. *Nature* **2005**, *434*, 917–921.
(12) Rubinstein, W. S. Hereditary breast cancer: pathobiology, clinical translation, and potential for targeted cancer therapeutics. *Fam. Cancer* **2008**, *7*, 83–89.
(13) Opar, A. Novel anticancer strategy targets DNA repair. *Nat. Rev. Drug Discovery* **2009**, *8*, 437–438.
(14) Daniel, R. A.; Rozanska, A. L.; Thomas, H. D.; Mulligan, E. A.; Drew, Y.; Castelbuono, D. J.; Hostomsky, Z.; Plummer, E. R.; Boddy, A. V.; Tweddle, D. A. Inhibition of poly (ADP-ribose) polymerase-1 enhances temozolomide and topotecan activity against childhood neuroblastoma. *Clin. Cancer Res.* **2009**, *15*, 1241–1249.
(15) Donawho, C. K.; Luo, Y.; Luo, Y.; Penning, T. D.; Bauch, J. L.; Bouska, J. J.; Bontcheva-Diaz, V. D.; Cox, B. F.; DeWeese, T. L.; Dillehay, L. E.; Ferguson, D. C.; Ghoreishi-Haack, N. S.; Grimm, D. R.; Guan, R.; Han, E. K.; Holley-Shanks, R. R.; Hristov, B.; Idler, K. B.; Jarvis, K.; Johnson, E. F.; Kleinberg, L. R.; Klinghofer, V.; Lasko, L. M.; Liu, X.; Marsh, K. C.; McGonigal, T. P.; Meulbroek, J. A.; Olson, A. M.; Palma, J. P.; Rodriguez, L. E.; Shi, Y.; Stavropoulos, J. A.; Tsurutani, A. C.; Zhu, G.-D.; Rosenberg, S. H.; Giranda, V. L.; Frost, D. J. ABT-888, an orally active poly(ADP-ribose) polymerase inhibitor that potentiates DNA-damaging agents in preclinical tumor models. *Clin. Cancer Res.* **2007**, *13*, 2728–2737.
(16) Penning, T. D.; Zhu, G.-D.; Gandhi, V. B.; Gong, J.; Liu, X.; Shi, Y.; Klinghofer, V.; Johnson, E. F.; Donawho, C. K.; Frost, D. J.; Bontcheva-Diaz, V.; Bouska, J. J.; Osterling, D. J.; Olson, A. M.; Marsh, K. C.; Luo, Y.; Giranda, V. L. Discovery of the

poly(ADP-ribose) polymerase (PARP) inhibitor 2-[(*R*)-2-methylpyrrolidin-2-yl]-1*H*-benzimidazole-4-carboxamide (ABT-888) for the treatment of cancer. *J. Med. Chem.* **2008**, *52*, 514–523.
(17) Thomas, H. D.; Calabrese, C. R.; Batey, M. A.; Canan, S.; Hostomsky, Z.; Kyle, S.; Maegley, K. A.; Newell, D. R.; Skalitzky, D.; Wang, L.-Z.; Webber, S. E.; Curtin, N. J. Preclinical selection of a novel poly(ADP-ribose) polymerase inhibitor for clinical trial. *Mol. Cancer Ther.* **2007**, *6*, 945–956.
(18) Plummer, R.; Lorigan, P.; Evans, J.; Steven, N.; Middleton, M.; Wilson, R.; Snow, K.; Dewji, R.; Calvert, H. First and final report of a phase II study of the poly(ADP-ribose) polymerase (PARP) inhibitor, AG014699, in combination with temozolomide (TMZ) in patients with metastatic malignant melanoma (MM). *J. Clin. Oncol.* **2006**, *24*, 8013.
(19) Peralta-Leal, A.; Rodriguez-Vargas, J. M.; Aguilar-Quesada, R.; Rodriguez, M. I.; Linares, J. L.; de Almodovar, M. R.; Oliver, F. J. PARP inhibitors: new partners in the therapy of cancer and inflammatory diseases. *Free Radical Biol. Med.* **2009**, *47*, 13–26.
(20) Jagtap, P.; Szab, C. Poly (ADP-ribose) polymerase and the therapeutic effects of its inhibitors. *Nat. Rev. Drug Discovery* **2005**, *4*, 421–440.
(21) Holbourn, K. P.; Shone, C. C.; Acharya, K. R. Exploring the mechanism of ADP-ribosylating toxins. *FEBS J.* **2006**, *273*, 4579–4593.
(22) Fieldhouse, R. J.; Merrill, A. R. Needle in the haystack: structure-based toxin discovery. *Trends Biochem. Sci.* **2008**, *33*, 546–556.
(23) Yates, S. P.; Merrill, A. R. A catalytic loop within *Pseudomonas aeruginosa* exotoxin A modulates its transferase activity. *J. Biol. Chem.* **2001**, *276*, 35029–35036.
(24) Roberts, T. M.; Merrill, A. R. A re-evaluation of the role of histidine-426 within *Pseudomonas aeruginosa* exotoxin A. *Biochem. J.* **2002**, *367*, 601–608.
(25) Armstrong, S.; Merrill, A. R. Toward the elucidation of the catalytic mechanism of the mono-ADP-ribosyltransferase activity of *Pseudomonas aeruginosa* exotoxin A. *Biochemistry* **2004**, *43*, 183–194.
(26) Parikh, S.; Schramm, V. Transition state structure for ADP-ribosylation of eukaryotic elongation factor 2 catalyzed by diphtheria toxin. *Biochemistry* **2004**, *43*, 1204–1212.
(27) Zhou, G.; Parikh, S.; Tyler, P.; Evans, G.; Furneaux, R.; Zubkova, O.; Benjes, P.; Schramm, V. Inhibitors of ADP-ribosylating bacterial toxins based on oxacarbenium ion character at their transition states. *J. Am. Chem. Soc.* **2004**, *126*, 5690–5698.
(28) Jorgensen, R.; Merrill, A. R.; Yates, S. P.; Marquez, V. E.; Schwan, A. L.; Boesen, T.; Andersen, G. R. Exotoxin A-eEF2 complex structure indicates ADP ribosylation by ribosome mimicry. *Nature* **2005**, *436*, 979–984.
(29) Jorgensen, R.; Wang, Y.; Visschedyk, D.; Merrill, A. R. The nature and character of the transition state for the ADP-ribosyltransferase reaction. *EMBO Rep.* **2008**, *9*, 802–809.
(30) Yates, S. P.; Taylor, P. L.; Jørgensen, R.; Ferraris, D.; Zhang, J.; Andersen, G. R.; Merrill, A. R. Structure−function analysis of water-soluble inhibitors of the catalytic domain of exotoxin A from *Pseudomonas aeruginosa*. *Biochem. J.* **2005**, *385*, 667–675.
(31) Jagtap, P.; Soriano, F. G.; Virág, L.; Liaudet, L.; Mabley, J.; Szabó, É.; Haskó, G.; Marton, A.; Lorigados, C. B.; Gallyas, F., Jr.; Sümegi, B.; Hoyt, D. G.; Baloglu, E.; VanDuzer, J.; Salzman, A. L.; Southan, G. J.; Szabó, C. Novel phenanthridinone inhibitors of poly(adenosine 5′-diphosphate-ribose) synthetase: potent cytoprotective and antishock agents. *Crit. Care Med.* **2002**, *30*, 1071–1082.
(32) Soriano, F. G.; Vir, g, L.; Jagtap, P.; Szab; Mabley, J. G.; Liaudet, L.; Marton, A.; Hoyt, D. G.; Murthy, K. G. K.; Salzman, A. L. Diabetic endothelial dysfunction: the role of poly (ADP-ribose) polymerase activation. *Nat. Med.* **2001**, *7*, 108–113.
(33) Yates, S.; Jorgensen, R.; Andersen, G.; Merrill, A. Stealth and mimicry by deadly bacterial toxins. *Trends Biochem. Sci.* **2006**, *31*, 123–133.
(34) Domenighini, M.; Rappuoli, R. Three conserved consensus sequences identify the NAD-binding site of ADP-ribosylating enzymes, expressed by eukaryotes, bacteria and T-even bacteriophages. *Mol. Microbiol.* **1996**, *21*, 667–674.
(35) Han, S.; Arvai, A. S.; Clancy, S. B.; Tainer, J. A. Crystal structure and novel recognition motif of rho ADP-ribosylating C3 exoenzyme from *Clostridium botulinum*: structural insights for recognition specificity and catalysis. *J. Mol. Biol.* **2001**, *305*, 95–107.
(36) Lehtio, L.; Jemth, A. S.; Collins, R.; Loseva, O.; Johansson, A.; Markova, N.; Hammarström, M.; Flores, A.; Holmberg-Schiavone, L.; Weigelt, J.; Helleday, T.; Schüler, H.; Karlberg, T. Structural basis for inhibitor specificity in human poly(ADP-ribose) polymerase-3. *J. Med. Chem.* **2009**, *52*, 3108–3111.
(37) Tsuge, H.; Nagahama, M.; Nishimura, H.; Hisatsune, J.; Sakaguchi, Y.; Itogawa, Y.; Katunuma, N.; Sakurai, J. Crystal structure and site-directed mutagenesis of enzymatic components from *Clostridium perfringens* iota-toxin. *J. Mol. Biol.* **2003**, *325*, 471–483.
(38) Bell, C. E.; Yeates, T. O.; Eisenberg, D. Unusual conformation of nicotinamide adenine dinucleotide (NAD) bound to diphtheria toxin: a comparison with NAD bound to the oxidoreductase enzymes. *Protein Sci.* **1997**, *6*, 2084–2096.
(39) Szabo, C.; Dawson, V. L. Role of poly (ADP-ribose) synthetase in inflammation and ischaemia−reperfusion. *Trends Pharmacol. Sci.* **1998**, *19*, 287–298.
(40) Yan, Z.; Yang, D. C. H.; Jett, M. Cholera toxin induces tumor necrosis factor α production in human monocytes. *Mol. Cell Biol. Res. Commun.* **1999**, *2*, 124–130.
(41) Griffin, R. J.; Srinivasan, S.; Bowman, K.; Calvert, A. H.; Curtin, N. J.; Newell, D. R.; Pemberton, L. C.; Golding, B. T. Resistance-modifying agents. 5. Synthesis and biological properties of quinazolinone inhibitors of the DNA repair enzyme poly(ADP-ribose) polymerase (PARP). *J. Med. Chem.* **1998**, *41*, 5247–5256.
(42) Skalitzky, D. J.; Marakovits, J. T.; Maegley, K. A.; Ekker, A.; Yu, X.-H.; Hostomsky, Z.; Webber, S. E.; Eastman, B. W.; Almassy, R.; Li, J.; Curtin, N. J.; Newell, D. R.; Calvert, A. H. Tricyclic benzimidazoles as potent poly(ADP-ribose) polymerase-1 inhibitors. *J. Med. Chem.* **2003**, *46*, 210–213.
(43) Liu, S. K.; Coackley, C.; Bristow, R. A novel poly (ADP-ribose) polymerase inhibitor, ABT-888, sensitizes malignant human cell lines to ionizing radiation under oxia and hypoxia. *Int. J. Radiat. Oncol., Biol., Phys.* **2007**, *69*, 615–615.
(44) Costantino, G.; Macchiarulo, A.; Camaioni, E.; Pellicciari, R. Modeling of poly (ADP-ribose) polymerase (PARP) inhibitors. Docking of ligands and quantitative structure−activity relationship analysis. *J. Med. Chem.* **2001**, *44*, 3786–3794.
(45) Zhang, C.; Liu, S.; Zhou, H.; Zhou, Y. An accurate, residue-level, pair potential of mean force for folding and binding based on the distance-scaled, ideal-gas reference state. *Protein Sci.* **2004**, *13*, 400–411.
(46) Zhang, C.; Liu, S.; Zhu, Q.; Zhou, Y. A knowledge-based energy function for protein−ligand, protein−protein, and protein−DNA complexes. *J. Med. Chem.* **2005**, *48*, 2325–2335.
(47) Brooks, B. R.; Bruccoleri, R. E.; Olafson, B. D.; States, D. J.; Swaminathan, S.; Karplus, M. CHARMm: a program for macromolecular energy, minimization, and dynamics calculations. *J. Comput. Chem.* **1983**, *4*, 187–217.
(48) MacKerell, J. A. D.; Bashford, D.; Bellott; Dunbrack, , R. L.; Evanseck, J. D.; Field, M. J.; Fischer, S.; Gao, J.; Guo, H.; Ha, , S.; Joseph-McCarthy, D.; Kuchnir, L.; Kuczera, K.; Lau, F. T. K.; Mattos, C.; Michnick, S.; Ngo, T.; Nguyen, D. T.; Prodhom, B.; Reiher, W. E.; Roux, B.; Schlenkrich, M.; Smith, J. C.; Stote, R.; Straub, J.; Watanabe, M.; Wiorkiewicz-Kuczera, J.; Yin, D.; Karplus, M. All-hydrogen empirical potential for molecular modeling and dynamics studies of proteins using the CHARMM22 force field. *J. Phys. Chem. B* **1998**, *102*, 3586–3616.
(49) Pavelites, J. J.; Gao, J.; Bash, P. A.; Mackerell, A. D., Jr. A molecular mechanics force field for NAD+, NADH, and the pyrophosphate groups of nucleotides. *J. Comput. Chem.* **1997**, *18*, 221–239.
(50) Jorgensen, W. L.; Chandrasekhar, J.; Madura, J. D.; Impey, R. W.; Klein, M. L. Comparison of simple potential functions for simulating liquid water. *J. Chem. Phys.* **1983**, *79*, 926–935.
(51) Allen, M. P.; Tildesley, D. J. *Computer Simulation of Liquids*; Oxford University Press: New York, 1987.
(52) Ryckaert, J. P.; Ciccotti, G.; Berendsen, H. J. C. Numerical integration of the Cartesian equations of motion of a system with constraints: molecular dynamics of *n*-alkanes. *J. Comput. Phys.* **1977**, *23*, 327–341.